Limitation of stochastic rotation dynamics to represent hydrodynamic interaction between colloidal particles

Ali Shakeri, Kuang-Wu Lee, and Thorsten Pöschel
Institute for Multiscale Simulations, Friedrich-Alexander-Universität, Erlangen, Germany

(Received 10 October 2017; accepted 2 January 2018; published online 24 January 2018)

Stochastic Rotation Dynamics (SRD) is a valuable numerical tool extensively used in many domains of hydrodynamics simulations including colloidal suspensions. We investigate the dynamics of two colloidal particles in the regime of low Reynolds number by means of SRD in 3D. In contrast to well-known analytical and experimental results, no long-range interaction between the suspended particles could be found, independent of the size of the particles and the Mach and Péclet numbers. We attribute this behavior to the compressible nature and low sound velocity in the SRD solvent. The inability of representing long-range interactions poses an important limitation to the applicability of SRD to certain physical systems. We provide an estimation of typical length scales for which SRD can be applied. *Published by AIP Publishing.* https://doi.org/10.1063/1.5008812

I. INTRODUCTION

Stochastic Rotation Dynamics (SRD) introduced by Malevanets and Kapral[1] is a widely used simulation method for the particle-based numerical simulation of fluids; thus, SRD belongs to the class of particle-based methods for computational fluid dynamics (CFD) simulations. In comparison with traditional lattice-based CFD, particle-based methods reveal a number of interesting features, which are of advantage in certain domains of fluid mechanics, in particular, for applications where thermal fluctuations are important. SRD was successfully applied to simulations of polymers,[2–4] suspensions of self-propelled particles,[5–7] dynamics of membranes,[8] and living cells.[9–11] By now, there is a large number of variants and extensions of the original SRD scheme[1] regarding incorporation of physical properties such as nonideal equations of state,[12] immiscible fluids,[13] angular momentum conservation,[14] surface wettability,[15] and isotropic collision rule.[16] Recent reviews on SRD and its applications can be found in Refs. 17 and 18.

In particular, SRD was applied to colloidal suspensions, e.g., Refs. 19 and 20. While many aspects of the dynamics of colloids could be modeled successfully, in the present paper, we will identify an important limitation of SRD which possibly restricts its applicability to colloids: The dynamics of colloidal suspensions are affected significantly by hydrodynamic interaction between the suspended particles. A prominent example is the slow sedimentation of particles in a fluid. For a dilute suspension of identical spheres, Batchelor[21] obtained the mean sedimentation velocity, $U = U_0(1 - \alpha\phi + \mathcal{O}(\phi^2))$, in the limit of the small volume fraction of the spheres, ϕ, where U_0 is the sedimentation velocity of a single sphere moving in an infinitely extended fluid and $\alpha = \alpha_{\text{flow}} + \alpha_{\text{int}} = 6.55$ is independent of the fluid's properties. Its main contribution, $\alpha_{\text{flow}} = 5$, comes from the reduction of the sedimentation velocity due to the upward flow of fluid caused by the downward motion of the spheres. The other contribution, $\alpha_{\text{int}} = 1.55$, is due to the hydrodynamic interaction of the spheres.[21] Another example of the effect of hydrodynamic interaction between suspended particles is the change in bulk stress of a suspension. Here the viscosity increases with the volume fraction due to diffusion and hydrodynamic forces between particles,[22] $\eta = \eta_0\left(1 + 2.5\phi + 6.2\phi^2\right)$, where η_0 is the viscosity of the pure solvent.

There are several investigations in the literature studying systems by means of SRD which are considerably affected by hydrodynamic interactions of suspended particles, e.g., Refs. 19, 23, and 24; however, by now, there is no systematic study regarding the range of reliability of SRD for the simulation of such systems, in particular, in regard of long-range hydrodynamic interactions. In this paper, we apply SRD to investigate the interaction between two spherical colloids in a solvent. We will show that long-range hydrodynamic interaction between the suspended particles is not sufficiently described which, thus, provides a limitation of the applicability of SRD to certain physical systems. Based on our findings, we provide an estimation of typical length scales for which SRD can be applied.

II. SRD SIMULATION SCHEME

A. Fluid dynamics

We consider a fluid in interaction with colloidal spheres in the absence of external forces. It is assumed that at any time the spheres are distant enough such that they do not interact *directly* with one another. Therefore, for the description of the algorithm, we restrict ourselves to a single colloidal particle in a fluid. For the SRD simulation (see, e.g., Ref. 17), the fluid is represented by N particles of mass m at positions $\vec{r}_i$ traveling at velocities $\vec{v}_i$. The radius, mass, position, and velocity of the colloidal particle are denoted by Λ, M, $\vec{R}$, and $\vec{V}$, respectively.

For each time step of the simulation, Δt, the fluid particles undergo a *streaming step* and a *collision step*. In case particle i does not collide with the colloidal particle during the current time step, the streaming step propagates the particle to its new

position according to its current velocity. The velocity of the particle is not changed by the streaming step,

$$\begin{aligned}\vec{r}_i(t+\Delta t) &= \vec{r}_i(t) + \Delta t\,\vec{v}_i(t),\\ \vec{v}_i^{\,s}(t+\Delta t) &= \vec{v}_i(t).\end{aligned} \tag{1}$$

In case particle i collides with the colloidal particle during the current time step, at time t^* (counted from the beginning of the current time step) with $t^* < \Delta t$, we employ a *bounce-back rule* to model a no-slip boundary condition for the interaction between a colloidal particle and the solvent: First, we determine the location at time t^* when the collision takes place,

$$\vec{r}_i(t^*) = \vec{r}_i(t) + t^*\,\vec{v}_i(t) \quad \text{with} \quad \left|\vec{r}_i(t^*) - \vec{R}\right| = \Lambda. \tag{2}$$

The collision corresponds to a transfer of momentum, $\Delta\vec{p}_i$, which at time t^* changes the velocities of both the fluid particle, i, and the colloidal particle. Therefore, the streaming step results in

$$\begin{aligned}\vec{r}_i(t+\Delta t) &= \vec{r}_i(t) + t^*\,\vec{v}_i(t) + (\Delta t - t^*)\left(\vec{v}_i - \frac{\Delta\vec{p}_i}{m}\right),\\ \vec{v}_i^{\,s}(t+\Delta t) &= \vec{v}_i - \frac{\Delta\vec{p}_i}{m}.\end{aligned} \tag{3}$$

By using energy conservation and considering no-slip boundary condition,[25] the transferred momentum, $\Delta\vec{p}_i$, becomes

$$\begin{aligned}\Delta\vec{p}_i = {}& 2\mu\left(\vec{v}_n - \vec{V}_n\right)\\ &+ 2\mu\frac{M\chi}{\mu + M\chi}\left[\vec{v}_t - \vec{V}_t - \Lambda\left(\vec{\Omega}\times\vec{n}\right)\right],\end{aligned} \tag{4}$$

where the indices n and t refer to the components normal and tangential to the colloidal particle's surface at the collision point, $\vec{n}$ is the inter-center unit vector between the colloidal particle and the fluid particle at the collision point, $\mu \equiv mM/(M + m)$ is the reduced mass, Ω is the angular velocity of the colloidal particle, and $\chi = \frac{2}{5}$. Note that the derivation of Eq. (4) requires some assumptions which are discussed in the Appendix.

The subsequent collision step rotates the fluctuating component of the velocities in dependence on the local temperature. To this end, we subdivide the simulation domain of size L, by means of a cubic grid of cell size a. Thus, each cell contains $\gamma = N(a/L)^3$ fluid particles, on average. The collision step reads then

$$\begin{aligned}\vec{v}_i(t+\Delta t) = {}& \left\langle\vec{v}^{\,s}(t+\Delta t)\right\rangle_{c_i}\\ &+ \hat{\varrho}(\alpha)\left[\vec{v}_i^{\,s}(t+\Delta t) - \left\langle\vec{v}^{\,s}(t+\Delta t)\right\rangle_{c_i}\right],\ i = 1,\ldots,N,\end{aligned} \tag{5}$$

where $\left\langle\vec{v}^{\,s}(t+\Delta t)\right\rangle_{c_i}$ is the average velocity of the fluid particles residing in the same grid cell as particle i after the streaming step. The matrix $\hat{\varrho}(\alpha)$ rotates the velocity vector by the constant angle, α, around a randomly chosen axis.[26] To ensure Galilean invariance, before each collision step, all particles are shifted by a vector whose components are chosen randomly from the interval $[-a/2, a/2]$. After performing the collision step, the particles are shifted back to their previous positions by the inverse vector.[27,28]

B. Solvent-particle interaction

A colloidal particle is modeled by a rigid sphere of radius Λ, mass $M = \frac{4}{3}\pi(\Lambda/a)^3\gamma m$, and moment of inertia, $I = \frac{2}{5}M\Lambda^2$. Note that the mass is chosen such that the density of the fluid and the sphere is the same. The positions, velocities, and angular velocities of the colloidal particles evolve due to the momenta transferred by the fluid particles given in Eq. (4),

$$\vec{R}(t+\Delta t) = \vec{R}(t) + \Delta t\,\vec{V}(t), \tag{6}$$

$$\vec{V}(t+\Delta t) = \vec{V}(t) + \frac{1}{M}\sum_i \Delta\vec{p}_i, \tag{7}$$

$$\vec{\Omega}(t+\Delta t) = \vec{\Omega}(t) + \frac{\Lambda}{I}\sum_i \vec{n}_i\times\Delta\vec{p}_i. \tag{8}$$

The summation in Eqs. (7) and (8) is performed for all fluid particles which collide with the colloidal particle in the current time step. This description refers to a single colloidal particle in a bath of fluid particles. Since the colloidal particles do not interact directly, all colloidal particles are handled in the same way, in case more than one is present.

III. SYSTEM CHARACTERISTICS

A. Units and dimensionless numbers

From the unit of length, a, characterizing the resolution of the hydrodynamic fields, unit of energy, k_BT, and mass, m, we obtain the unit of time, $t_0 \equiv a\sqrt{m/k_BT}$, and kinematic viscosity, $\nu_0 \equiv a^2/t_0$. The dimensionless mean free path[29] can then be defined as the average displacement of fluid particles due to streaming in units of a,

$$\lambda \equiv \frac{\Delta t}{a}\sqrt{\frac{k_BT}{m}} = \frac{\Delta t}{t_0}. \tag{9}$$

The choice of $\alpha = \pi/2$ along with an average of 10 particles per cell leads to the kinematic viscosity, $\nu \approx \frac{0.05}{\lambda}\nu_0$, and self-diffusion of a fluid particle, $D_f \approx 1.17\lambda\nu_0$.[29]

In this paper, we consider a flow at a small Reynolds number, small Knudsen number, and large Schmidt number, which all correspond to small mean free path. Therefore, in all simulations presented, we chose the time step size corresponding to small values of λ, see Table I.

TABLE I. Set of dimensionless numbers due to the parameters of the simulations. The last three columns refer to the set of parameters used in Sec. IV. The average velocity of a colloidal particle is obtained from the equipartition of energy, $U = \sqrt{3k_BT/M}$; $C = \sqrt{\frac{5}{3}k_BT/m}$ is the speed of sound, and D_0 is the colloid self diffusion coefficient [see Eq. (13)].

		$\Lambda = 2a$, $\lambda = 0.05$	$\Lambda = 3a$, $\lambda = 0.02$	$\Lambda = 4a$, $\lambda = 0.02$
Reynolds	$\mathrm{Re} = \frac{U\Lambda}{\nu}$	0.2	0.06	0.05
Mach	$\mathrm{Ma} = \frac{U}{C}$	0.07	0.04	0.03
Knudsen	$\mathrm{Kn} = \frac{\lambda}{\Lambda}$	0.025	0.007	0.005
Péclet	$\mathrm{Pe} = \frac{U\Lambda}{D_0}$	73	223	249
Schmidt	$\mathrm{Sc} = \frac{\nu}{D_f}$	17	107	107

B. Hierarchy of time scales

For the description of colloidal systems on the hydrodynamic level, it is assumed that perturbations of the equilibrium state propagate and relax much faster than the time scale of measurements, that is, they propagate instantaneously throughout the system without any delay.[30] On the mesoscopic level considered in particle-based fluid mechanics such as SRD, however, the propagation of any information takes finite time mainly determined by the speed of sound. In order to achieve a physically meaningful hierarchy of time scales, the simulation parameters characterizing the fluid properties and measurement intervals must be carefully chosen. Table II summarizes the characteristic time scales relevant for our system.

Density perturbations in a fluid propagate due to two mechanisms: *shear waves* are of transverse nature and *sound wave* or pressure wave propagating pressure differences are longitudinal.[30] The *hydrodynamic* scale, $\tau_H \equiv \frac{\Lambda^2}{\nu}$, is given by the time it takes a shear wave to travel one radius of the colloidal particle. Similarly, the *sonic* scale, $\tau_c \equiv \frac{\Lambda}{C}$, is the time it takes a sound wave to travel one radius, where C is the speed of sound, see Table II. The motion of the colloidal particle can be ballistic or diffusive depending on the time resolution of the measurement of its position. This defines the *Brownian* time scale, $\tau_B \equiv \frac{M}{6\pi\eta\Lambda}$, separating ballistic from diffusive behaviors. Since the density of Brownian particles is usually similar to the density of the fluid, the Brownian time scale is of the same order as the hydrodynamic time scale, $\tau_B \approx \tau_H$.

Finally, there is the *experimental* time scale, τ_{exp}, defined by the rate at which positions of the colloidal particles are measured. This time scale should be larger than the sonic and kinematic time scales in order to allow interactions mediated by the fluid to propagate between the colloidal particles. For a 1 μm colloidal particle in water, the hierarchy of time scales is $\tau_c \ll \tau_H$, $\tau_B \ll \tau_{exp}$, see the last column of Table II.

In the simulation, the units of length, a, mass, m, and energy, k_BT, are chosen unity which implies that the unit of time, t_0, is unity too. The correspondence to physical quantities is obtained by appropriately choosing the SRD simulation parameters, which are the number of fluid particles per cell, γ, the rotation angle, α, and the dimensionless mean free path, λ. The physical transport coefficients and the SRD simulation parameters are then related via

$$D_f = \lambda\left[\frac{3}{2(1-\cos\alpha)}\frac{\lambda}{\lambda-1}-\frac{1}{2}\right]\frac{a^2}{t_0}, \tag{10}$$

$$\nu = \left[\lambda\left(\frac{5\gamma}{(\gamma-1+e^{-\gamma})(4-2\cos\alpha-2\cos 2\alpha)}-\frac{1}{2}\right) + \frac{(1-\cos\alpha)\left(1-\frac{1}{\gamma}+\frac{e^{-\gamma}}{\gamma}\right)}{18\lambda}\right]\frac{a^2}{t_0}. \tag{11}$$

For the choice $\alpha = \frac{\pi}{2}$, $\gamma = 10$, as typical for SRD simulations, we obtain the transport coefficients as functions of the mean free path, λ,

$$D_f \approx 1.167\lambda\frac{a^2}{t_0}, \qquad \nu \approx \left(0.426\lambda + \frac{0.05}{\lambda}\right)\frac{a^2}{t_0}. \tag{12}$$

The value of λ follows from the chosen time step, see Eq. (9). To obtain realistic material characteristics, it may be desirable to choose small values of λ. For physical reasons, however, due to the discussion above, we are not free to choose arbitrary values of λ in order to assure the hierarchy of time scales in the simulation since the time scales depend on λ, see the second column of Table II. In particular, the value of λ cannot be chosen too small; otherwise the sonic scale, τ_c, would exceed the hydrodynamic scale, τ_H. Thus, the condition $\tau_H/\tau_c \sim 1$ provides a limit for the choice of λ. In colloidal systems, typically $\tau_H/\tau_c \sim 10^3$, see the last column in Table II.

TABLE II. Hierarchy of characteristic time scales. For a detailed description, see the text. The columns $\Lambda = 2a$, $\Lambda = 3a$, and $\Lambda = 4a$ refer to the sizes of the colloidal particles used in Sec. IV. The last column gives the time scales for colloidal particles of radius 1 μm dispersed in water in units of seconds.

		$\Lambda = 2a$, $\lambda = 0.05$ (t_0)	$\Lambda = 3a$, $\lambda = 0.02$ (t_0)	$\Lambda = 4a$, $\lambda = 0.02$ (t_0)	1 μm colloid in water (s)
τ_c	$\frac{\Lambda}{C}$	1.6	2.3	3.1	10^{-9}
τ_H	$\frac{\Lambda^2}{\nu}$	4	3.6	6.4	10^{-6}
τ_B	$\frac{\Lambda^2}{\nu}$	4	3.6	6.4	10^{-6}
τ_{exp}		8	8	10	10^{-2}

C. Two-particle dynamics

For a single spherical colloidal particle, diffusion is isotropic and is, thus, characterized by a scalar coefficient of diffusion given by the Stokes-Einstein relation,

$$D_0 = \frac{k_BT}{6\pi\eta\Lambda}. \tag{13}$$

We measure the diffusion coefficient of a single colloidal particle by calculating mean square displacement, $\langle[\vec{R}(t)-\vec{R}(0)]^2\rangle = 6D_0t$, where $\vec{r}(t)$ is the position of the colloidal particle at time t. To measure the diffusion coefficient, time intervals for position measurements have to be greater than τ_H; otherwise, we see the ballistic behavior. For $t \ll \tau_H$, the mean square displacement is $\langle[\vec{R}(t)-\vec{R}(0)]^2\rangle = \vec{V}(0)\mathbf{V}(0)t^2 = \frac{3k_BT}{M}t^2$.[30] Figure 1 shows ballistic and diffusive regimes for a colloid of size $\Lambda = 4a$ in an SRD fluid with $\lambda = 0.02$.

Considering the motion of a pair of colloidal particles, the dynamics is described by the motion of the center of mass (collective motion) and by the relative motion of the particles. Both types of motion are of broken symmetry, characterized by the direction of the inter-center unit vector, $\vec{e}$. Correspondingly, the diffusive behavior is described by four coefficients describing diffusive motion which are functions of the dimensionless

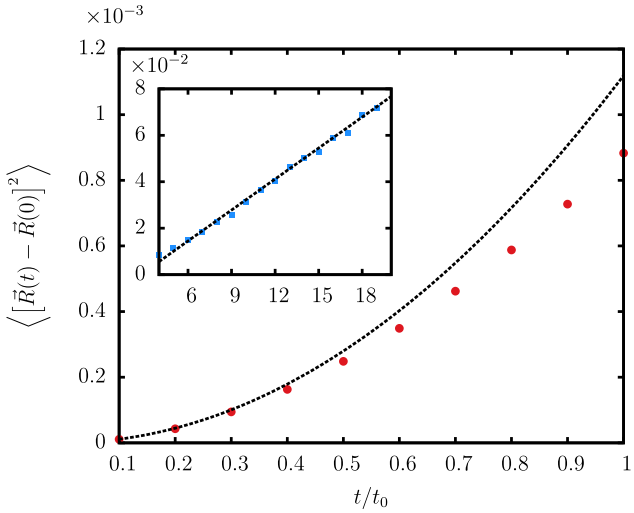

FIG. 1. Mean square displacement for a single colloidal particle as a function of time. Main figure: For short time scales, $t \lesssim \tau_H$, the colloidal particle shows ballistic behavior. The dashed line shows the function $\langle[\vec{R}(t) - \vec{R}(0)]^2\rangle = \frac{3k_BT}{M}t^2$. Inset: for large time, diffusive motion is observed. The dashed line is a linear fit to the simulation data. From the slope, we obtain the coefficient of diffusion via $\langle[\vec{R}(t) - \vec{R}(0)]^2\rangle = 6D_0\,t$.

separation of the colloidal particles, $\rho = |\vec{R}_2 - \vec{R}_1|/\Lambda$.[31] Two coefficients describe the relative motion,

$$D^{\parallel}_{\mathrm{rm}} = \frac{D_0}{2}\left[1 - \frac{3}{2\rho} + \frac{1}{\rho^3} - \frac{15}{4\rho^4} + \mathcal{O}\left(\rho^{-6}\right)\right],$$

$$D^{\perp}_{\mathrm{rm}} = \frac{D_0}{2}\left[1 - \frac{3}{4\rho} - \frac{1}{2\rho^3} + \mathcal{O}\left(\rho^{-6}\right)\right], \tag{14}$$

and two describe the collective motion,

$$D^{\parallel}_{\mathrm{cm}} = \frac{D_0}{2}\left[1 + \frac{3}{2\rho} - \frac{1}{\rho^3} - \frac{15}{4\rho^4} + \mathcal{O}\left(\rho^{-6}\right)\right],$$

$$D^{\perp}_{\mathrm{cm}} = \frac{D_0}{2}\left[1 + \frac{3}{4\rho} + \frac{1}{2\rho^3} + \mathcal{O}\left(\rho^{-6}\right)\right]. \tag{15}$$

The coefficients $D^{\parallel}_{\mathrm{rm}}$ and $D^{\parallel}_{\mathrm{cm}}$ characterize the diffusion in the direction of $\vec{e}$; the other two, $D^{\perp}_{\mathrm{rm}}$ and $D^{\perp}_{\mathrm{cm}}$, characterize the diffusion in the plane perpendicular to $\vec{e}$. The theoretical prediction by Batchelor, Eqs. (14) and (15), for the hydrodynamic coupling between two spheres was experimentally confirmed by Crocker.[31]

IV. RESULTS AND DISCUSSION

We did several tests to make sure that we can reproduce important results that usually are used as SRD benchmarks. First, we tested three-dimensional Poiseuille flow between two parallel walls with no-slip boundaries, and our results are in agreement with those of Allahyarov *et al.*[26] We also measured the transport coefficients for our three-dimensional fluid, and our results are consistent with the work of Padding[29]. In order to check the no-slip boundary on colloid's surface, we measured translational and rotational velocity autocorrelation functions. The short-time and long-time behavior agrees well with Enskog kinetic theory and hydrodynamic mode-coupling theory, respectively.[32]

We consider the pair diffusion of two colloidal particles of radius Λ as a function of their dimensionless separation, ρ, in a cubic box of size L with periodic boundary conditions. The ratio $L/\Lambda = 25$ was kept constant for all simulations, in order to exclude finite size effects for different sizes of the colloidal particle.[29] The fluid is represented by $N = 10^6, \ldots, 10^7$ fluid particles homogeneously distributed in the simulation domain by avoiding the space occupied by the colloidal particles; thus, each cell of the simulation grid contains 10 fluid particles on average. During the simulation, the distance between the surfaces of the colloidal particles did not fall below $a/2$ which corresponds to a minimum of 385 fluid particles populating the region between the colloidal particles, see Fig. 2.

Since there is no direct force acting between colloidal particles, hydrodynamic interaction is the only coupling. This hydrodynamic coupling is due to the resistance of the fluid between the colloidal particles against the relative motion of the colloidal particles in the relative normal and tangential directions.

For the system described earlier, we compare the simulation results with the analytical expressions, Eqs. (14) and (15), by the following procedure: Starting from their initial positions, after disregarding the time τ_{exp} to exclude the influence of the initial state, the traces of the colloidal particles, $\vec{R}_1(t)$ and $\vec{R}_2(t)$, have been recorded. Whenever the distance of the surfaces of the colloidal particles fell below $a/2$, the simulation was restarted from the initial state. By this procedure, we gathered about 5×10^6 pairs $(\vec{R}_1, \vec{R}_2)$. From these time series of particle positions, we compute the trajectories of collective and relative motion,

$$\vec{X}_{\mathrm{cm}}(t) = \frac{\vec{R}^*_1(t) + \vec{R}^*_2(t)}{2}, \tag{16}$$

$$\vec{X}_{\mathrm{rm}}(t) = \frac{\vec{R}^*_1(t) - \vec{R}^*_2(t)}{2}, \tag{17}$$

where

$$\vec{R}^*_i(t) \equiv \frac{1}{\tau_{\mathrm{exp}}}\int_{t-\tau_{\mathrm{exp}}}^{t} \vec{R}_i(t')\mathrm{d}t' \tag{18}$$

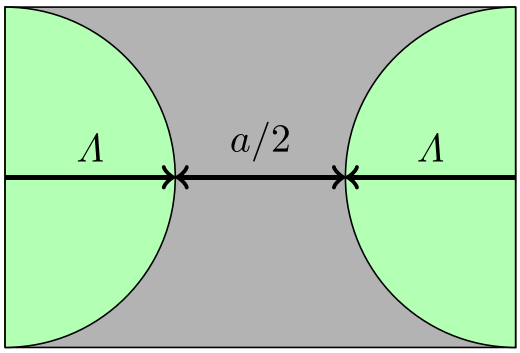

FIG. 2. The average number of fluid particles, $\bar{N}_{\mathrm{min}}$, between colloidal particles separated by $a/2$ follows from the inter-particle fluid volume, $4\Lambda^2(2\Lambda + a/2) - \frac{4}{3}\pi\Lambda^3$, and the particle number density, (10 particles/a^3). For the radius of the colloidal particle, $\Lambda = 2a, 3a, 4a$, we obtain $\bar{N}_{\mathrm{min}} \approx 385, 1209, 2759$.

is a smoothening running average and eventually the displacements

$$\begin{aligned}
\Delta X^{\parallel}_{\mathrm{cm}}(t,\tau) &= \left(\vec{X}_{\mathrm{cm}}(t+\tau) - \vec{X}_{\mathrm{cm}}(t)\right)\cdot\vec{e}(t),\\
\Delta X^{\perp}_{\mathrm{cm}}(t,\tau) &= \left|\vec{X}_{\mathrm{cm}}(t+\tau) - \vec{X}_{\mathrm{cm}}(t) - \Delta X^{\parallel}_{\mathrm{cm}}(\tau)\,\vec{e}(t)\right|,\\
\Delta X^{\parallel}_{\mathrm{rm}}(t,\tau) &= \left(\vec{X}_{\mathrm{rm}}(t+\tau) - \vec{X}_{\mathrm{rm}}(t)\right)\cdot\vec{e}(t),\\
\Delta X^{\perp}_{\mathrm{rm}}(t,\tau) &= \left|\vec{X}_{\mathrm{rm}}(t+\tau) - \vec{X}_{\mathrm{rm}}(t) - \Delta X^{\perp}_{\mathrm{rm}}(\tau)\,\vec{e}(t)\right|
\end{aligned} \tag{19}$$

with the inter-center unit vector $\vec{e}$ and with the side condition $\tau \geq \tau_{exp}$. In order to compute the diffusion coefficients, $D^{\parallel}_{\mathrm{cm}}$, $D^{\perp}_{\mathrm{cm}}$, $D^{\parallel}_{\mathrm{rm}}$, and $D^{\perp}_{\mathrm{rm}}$, as a function of the distance of the particles, $\rho \equiv |\vec{R}_1(t) - \vec{R}_2(t)|$, we select those pairs (t,τ) for which ρ falls in a certain interval, $|\rho^* - \rho| \leq \Delta\rho$, and fit straight lines to the mean square displacements as functions of τ,

$$\begin{aligned}
\left\langle\left(\Delta\vec{X}^{\parallel}_{\mathrm{cm}}(t,\tau)\right)^2\right\rangle\Big|_{|\rho^*-\rho|\leq\Delta\rho} &= 2D^{\parallel}_{\mathrm{cm}}(\rho^*)\,\tau,\\
\left\langle\left(\Delta\vec{X}^{\perp}_{\mathrm{cm}}(t,\tau)\right)^2\right\rangle\Big|_{|\rho^*-\rho|\leq\Delta\rho} &= 4D^{\perp}_{\mathrm{cm}}(\rho^*)\,\tau,\\
\left\langle\left(\Delta\vec{X}^{\parallel}_{\mathrm{rm}}(t,\tau)\right)^2\right\rangle\Big|_{|\rho^*-\rho|\leq\Delta\rho} &= 2D^{\parallel}_{\mathrm{rm}}(\rho^*)\,\tau,\\
\left\langle\left(\Delta\vec{X}^{\perp}_{\mathrm{rm}}(t,\tau)\right)^2\right\rangle\Big|_{|\rho^*-\rho|\leq\Delta\rho} &= 4D^{\perp}_{\mathrm{rm}}(\rho^*)\,\tau.
\end{aligned} \tag{20}$$

This calculation was performed for $\rho^* = \rho_0 + 2\,l\,\Delta\rho$, ($l = 0, 1, 2, \ldots$) with $\rho_0 = 2.5$ and $\Delta\rho = 0.1$.

Figure 3 shows the diffusion coefficients for three values of the size of the colloidal particles, Λ, corresponding to different Mach numbers, see Table I. In contrast to the results from hydrodynamics theory (red lines in Fig. 3), the simulation results do not reveal any evidence of hydrodynamic coupling of the colloidal particles. The insufficient description of long-range interaction results from the particulate nature of the SRD simulation method: In a real fluid, the time scale at which shear and sound waves propagate is small compared to the experimental time scale such that the approximation of instantaneous interactions exploited in hydrodynamics is justified.[30] This separation of time scales is not necessarily granted in mesoscopic simulations,[29] see Table II.

Further in SRD, the propagation of density perturbations is a purely diffusive process, similar to an ideal gas. This can be seen from the fact that the collision rate in SRD is independent of the local density, in contrast to physical fluids where the propagation of density perturbations is dominated by strong repulsion forces between the fluid particles. The compressible nature of SRD fluids cannot be avoided by increasing the number of simulated fluid particles and is independent of the Mach number.

The limitation of SRD can be quantified by studying the propagation of sound and shear waves which play an important role for the propagation of hydrodynamic interactions.[30] In a Newtonian fluid, the amplitude of a sound wave decays exponentially with the traveled distance.[33] The amplitude of a plane wave of angular frequency ω decreases by the factor $1/e$

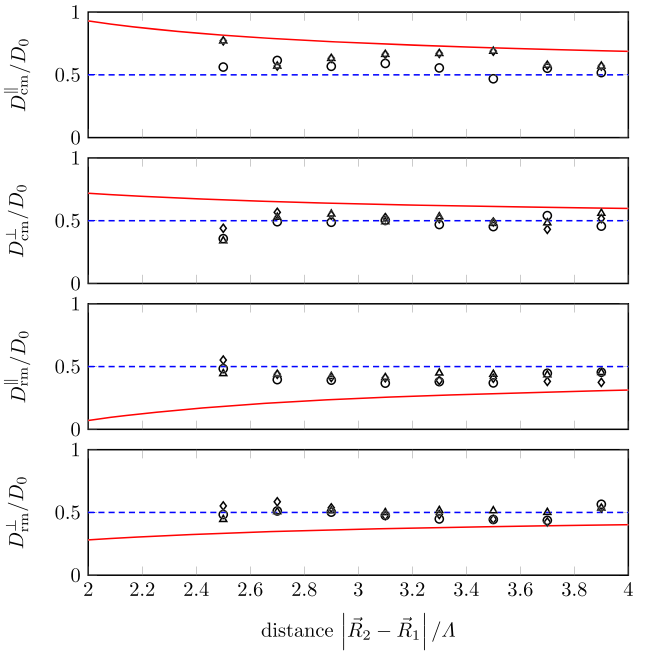

FIG. 3. The diffusion coefficients defined in Eqs. (14) and (15) as functions of the separation of the colloidal particles, normalized by the single-particle coefficient, D_0, see Eq. (13). The symbols stand for different values of the particle radius: $\Lambda = 2a$ (diamonds), $\Lambda = 3a$ (triangles), $\Lambda = 4a$ (circles). Red solid lines show the analytical expressions for incompressible fluids, Eqs. (14) and (15). Blue dashed lines are the values expected in the absence of any coupling between the colloidal particles.

after the decay length,

$$d = \frac{3C^3}{2\nu\omega^2}. \tag{21}$$

For ordinary viscous fluids like pure water, the decay length for a 1 MHz sound wave is of the order $d \sim 100$ m.[34] This means that for 1 μm particles in water, the decay length is 10^8 times larger than the particle size. To check the decay length for an SRD fluid, we consider a rectangular volume of size $(L_x/a, L_y/a, L_z/a) = (200, 200, 40)$ with periodic boundaries in the x and y directions and no-slip boundary conditions in the z direction. The x–y plane at $z = 0$ is oscillated sinusoidally in the x direction with amplitude $A = 0.1a$ and frequency ω

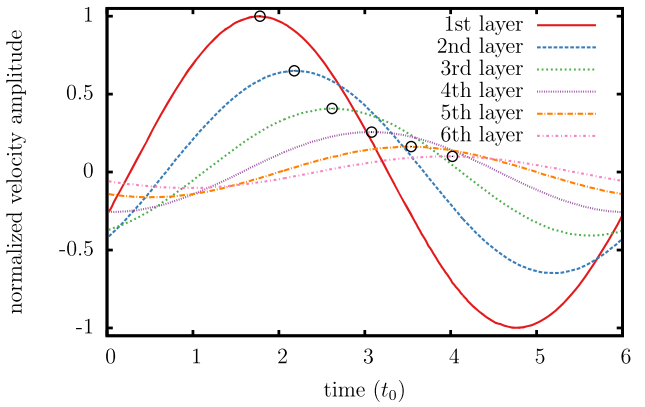

FIG. 4. Elongation of the shear wave over one period in different distances, D, from the wall obtained from SRD simulations. The amplitude (hollow circles) decreases with distance from the wall. The decay length is about $d \sim 2a$.

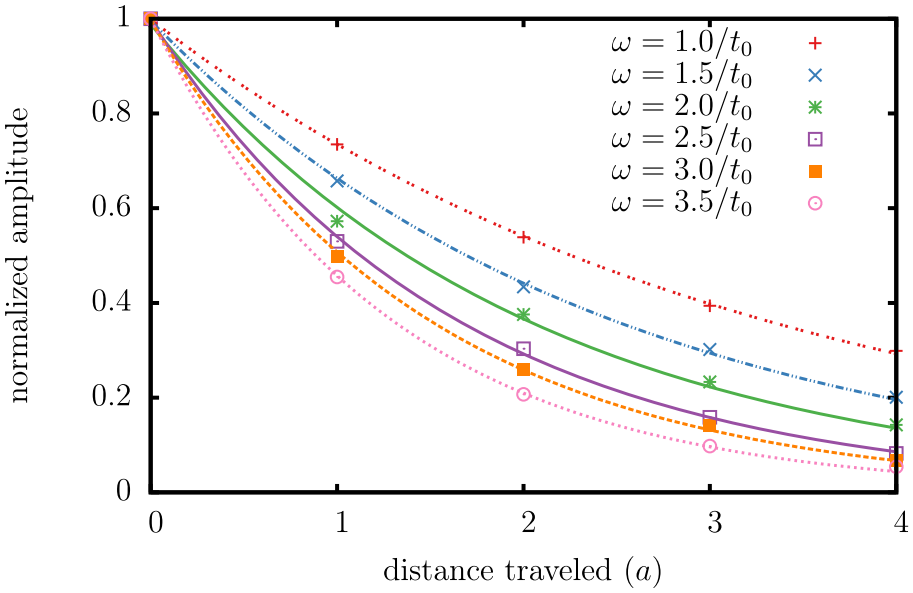

FIG. 5. Attenuation of the sound wave for different frequencies. Again, the decay length is in the order $d \sim 2a$, depending on the frequency as described by Eq. (21).

to excite shear waves. The typical values for frequency is of the order of $\frac{1}{\tau_B}$. Figure 4 shows the elongation of the shear wave over one period in different distances from the wall obtained from SRD simulations. Data have been recorded for $\omega = 1/t_0$ and viscosity $\nu = 2.51\nu_0$, after performing several periods such that transient effects due to the initial conditions have faded away. Hollow circles mark the amplitudes of the oscillation.

The attenuation of the sound wave was determined by the same setup, but the x–y plane at $z = 0$ is oscillated in the z direction. Figure 5 shows the normalized amplitude of the wave as a function of distance from the wall for $\omega \in (1-3.5)\frac{1}{t_0}$. The same data but for $\omega = 1/t_0$ and different viscosities are shown in Fig. 6. From the data shown in Figs. 5 and 6, we see that the decay lengths are orders of magnitude off the value obtained from hydrodynamics, Eq. (21). In order to obtain higher values for the decay length, the viscosity would have to be lowered by choosing appropriate values for the simulation time steps dt and the rotation angle, α, see Eq. (5). However, by lowering the viscosity, we are no longer in the low Reynolds regime.

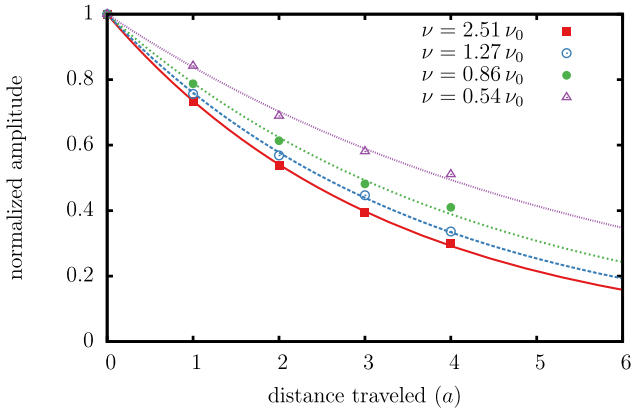

FIG. 6. Sound attenuation plotted for various viscosities. For higher viscosities, we observe faster decay since the fluid is more dissipative.

V. CONCLUSION

We challenge Stochastic Rotation Dynamics (SRD) by applying the method to a colloidal suspension. The hydrodynamic interaction of two spherical colloidal particles in a certain distance from one another is known from hydrodynamics theory[22] supported by experimental results.[31] In particular, we applied SRD to compute the pair diffusion coefficients and checked them against the theoretical results, Eqs. (14) and (15). Our numerical results reveal a significant deviation from theory; thus, the hydrodynamical interactions of colloidal particles are not sufficiently described by SRD. The results do not depend on the particle size, e.g., they are independent of the Mach number. We attribute this deviation to the incorrect modeling of the speed of sound and the viscosity of the solvent by SRD. This argument is supported by the decay length of induced sound and shear waves studied for an SRD fluid. Both decay lengths are in strong conflict with the decay lengths found for typical physical fluids. Although there are a number of simulation parameters, such as rotation angle, α, time step, Δt, and particle number density, to represent the characteristics of the fluid, we checked systematically that these parameters cannot be chosen (respecting the time scale hierarchy) such that long-range interactions are represented. Therefore, we do not believe that SRD can be applied to the simulation of systems where the long-range interaction is essential.

In summary, our results show that while SRD may be a valuable tool for hydrodynamical simulations in many practical cases, it fails for colloidal systems at low Reynolds numbers. Thus, obviously, an important part of the physics of fluids is not well modeled by SRD and further work is necessary to overcome this limitation.

ACKNOWLEDGMENTS

The authors gratefully acknowledge the support of the German Research Foundation (DFG) through the Cluster of Excellence “Engineering of Advanced Materials” (EXC-215)

and the Collaborative Research Center (SFB-814), FPS, and ZISC.

APPENDIX: DERIVATION OF EQ. (4)

Consider the collision of a point fluid particle traveling at velocity $\vec{v}$ with a colloidal particle of radius Λ moving at velocity $\vec{V}$ and angular velocity $\vec{\Omega}$. The corresponding post-collisional quantities are $\vec{v}'$, $\vec{V}'$, and $\vec{\Omega}'$. We define the relative velocity between the fluid particle and surface of the colloidal particle at the collision point,

$$\vec{g}_{ij} \equiv \vec{v} - \vec{V} - \Lambda\left(\vec{\Omega}\times\vec{n}\right), \tag{A1}$$

where $\vec{n}$ is the inter-center unit vector. Its projections to the directions normal and tangential to the colloid's surface are

$$\vec{g}_{ij}^{\,n} = \left(\vec{g}_{ij}\cdot\vec{n}\right)\vec{n}\,, \qquad \vec{g}_{ij}^{\,t} = -\vec{n}\times\left(\vec{n}\times\vec{g}_{ij}\right). \tag{A2}$$

The post-collisional quantities read

$$(\vec{g}_{ij}^{\,n})' = -\vec{g}_{ij}^{\,n}, \qquad (\vec{g}_{ij}^{\,t})' = \Gamma\vec{g}_{ij}^{\,t}. \tag{A3}$$

where the coefficient Γ is determined by the specific collision rule. For bounce back collisions corresponding to the no-slip boundary condition on the colloid's surface, $\Gamma = -1$ while for slip boundaries $\Gamma = 1$. Thus,

$$\left(\vec{g}_{ij}^{\,n}\right)' - \vec{g}_{ij}^{\,n} = -2\vec{g}_{ij}^{\,n}\,, \quad \left(\vec{g}_{ij}^{\,t}\right)' - \vec{g}_{ij}^{\,t} = (\Gamma-1)\vec{g}_{ij}^{\,t}. \tag{A4}$$

Further, we exploit the conservation of linear and angular momentum,

$$\begin{aligned} m\vec{v}\,' + M\vec{V}\,' &= m\vec{v} + M\vec{V}, \\ M\Lambda\left(\vec{n}\times\vec{V}\,'\right) - I\vec{\Omega}\,' &= M\Lambda\left(\vec{n}\times\vec{V}\right) - I\vec{\Omega}. \end{aligned} \tag{A5}$$

We define the momentum, $\Delta\vec{p}$, transferred to the colloidal particle due to the collision and rewrite Eqs. (A5),

$$\vec{v}\,' = \vec{v} - \frac{\Delta\vec{p}}{m}\,, \quad \vec{V}\,' = \vec{V} + \frac{\Delta\vec{p}}{M}\,, \quad \vec{\Omega}\,' = \vec{\Omega} + \frac{\Lambda}{I}\left(\vec{n}\times\Delta\vec{p}\,\right). \tag{A6}$$

With the reduced mass, μ, and $I \equiv \chi M\Lambda^2$, the post-collisional relative velocity at the point of contact is

$$\begin{aligned} \left(\vec{g}_{ij}\right)' &= \vec{v}\,' - \vec{V}\,' - \Lambda\left(\vec{\Omega}\,'\times\vec{n}\right) \\ &= \vec{v} - \frac{\Delta\vec{p}}{m} - \vec{V} - \frac{\Delta\vec{p}}{M} - \Lambda\left(\vec{\Omega}\times\vec{n}\right) + \frac{\Lambda^2}{I}\vec{n}\times\left(\vec{n}\times\Delta\vec{p}\,\right) \\ &= \vec{g}_{ij} - \frac{\Delta\vec{p}}{\mu} + \frac{1}{\chi M}\,\vec{n}\times\left(\vec{n}\times\Delta\vec{p}\,\right). \end{aligned} \tag{A7}$$

The components of $\vec{g}_{ij}' - \vec{g}_{ij}$ in the normal and tangential directions to the sphere's surface are then

$$\left[\vec{n}\cdot\left(\vec{g}_{ij}' - \vec{g}_{ij}\right)\right]\vec{n} = -\left(\vec{n}\cdot\frac{\Delta\vec{p}}{\mu}\right)\vec{n} = -\frac{\Delta\vec{p}_n}{\mu}, \tag{A8}$$

$$\begin{aligned} \vec{n}\times\left(\vec{g}_{ij}' - \vec{g}_{ij}\right) &= \vec{n}\times\left[-\frac{\Delta\vec{p}}{\mu} + \frac{1}{\chi M}\left\{\left(\vec{n}\cdot\Delta\vec{p}\,\right)\vec{n} - \Delta\vec{p}\,\right\}\right] \\ &= -\frac{1}{\mu}\left(\vec{n}\times\Delta\vec{p}\,\right) - \frac{1}{\chi M}\left(\vec{n}\times\Delta\vec{p}\,\right) \\ &= -\frac{\chi M+\mu}{\mu\chi M}\left(\vec{n}\times\Delta\vec{p}\,\right). \end{aligned} \tag{A9}$$

Multiplying both sides by $\vec{n}$, we find

$$\begin{aligned} -\vec{n}\times\left[\vec{n}\times\left(\vec{g}_{ij}' - \vec{g}_{ij}\right)\right] &= \frac{\chi M+\mu}{\mu\chi M}\,\vec{n}\times\left(\vec{n}\times\Delta\vec{p}\,\right) \\ &= -\frac{\chi M+\mu}{\mu\chi M}\,\Delta\vec{p}_t. \end{aligned} \tag{A10}$$

From Eqs. (A10), (A8), (A2), and (A4), we obtain eventually the components of $\Delta\vec{p}$, given in Eq. (4),

$$\begin{aligned} \Delta\vec{p}_n &= 2\mu\vec{g}_{ij}^{\,n} = 2\mu\left(\vec{v}_n - \vec{V}_n\right), \\ \Delta\vec{p}_t &= 2\mu\frac{\chi M}{\mu+\chi M}\vec{g}_{ij}^{\,t} = 2\mu\frac{\chi M}{\mu+\chi M}\left(\vec{v}_t - \vec{V}_t - \Lambda(\vec{\Omega}\times\vec{n})\right). \end{aligned} \tag{A11}$$

Finally, we will show that the derived expression for $\Delta\vec{p}$ satisfies the conservation of energy,

$$m\left(\vec{v}\,'^2 - \vec{v}^{\,2}\right) + M\left(\vec{V}\,'^2 - \vec{V}^{\,2}\right) + I\left(\vec{\Omega}\,'^2 - \vec{\Omega}^{\,2}\right) = 0. \tag{A12}$$

With Eqs. (A6), we obtain

$$\begin{aligned} \Delta\vec{p}\cdot\left(\vec{V} - \vec{v}\right) + \frac{\Delta\vec{p}^{\,2}}{2\mu} + \Lambda\vec{\Omega}\cdot\left(\vec{n}\times\Delta\vec{p}\,\right) \\ + \frac{1}{2\chi M}\left[\Delta\vec{p}^{\,2} - \left(\vec{n}\cdot\Delta\vec{p}\,\right)^2\right] = 0. \end{aligned} \tag{A13}$$

Rewriting the above equation using the components of $\Delta\vec{p} = \Delta\vec{p}_n + \Delta\vec{p}_t$, we obtain

$$\begin{aligned} &\left[\vec{V}_n - \vec{v}_n + \frac{\Delta\vec{p}_n}{2\mu}\right]\cdot\Delta\vec{p}_n + \\ &\left[\vec{V}_t - \vec{v}_t + \Lambda(\vec{\Omega}\times\vec{n}) + \frac{\Delta\vec{p}_t}{2\mu}\left(\frac{\chi M+\mu}{\chi M}\right)\right]\cdot\Delta\vec{p}_t = 0. \end{aligned} \tag{A14}$$

Inserting the derived expression, Eq. (A11), it can be checked that the conservation of energy is satisfied.

[1] A. Malevanets and R. Kapral, "Mesoscopic model for solvent dynamics," J. Chem. Phys. **110**, 8605–8613 (1999).
[2] K. Mussawisade, M. Ripoll, R. G. Winkler, and G. Gompper, "Dynamics of polymers in a particle-based mesoscopic solvent," J. Chem. Phys. **123**, 144905 (2005).
[3] S. H. Lee and R. Kapral, "Mesoscopic description of solvent effects on polymer dynamics," J. Chem. Phys. **124**, 214901 (2006).
[4] C.-C. Huang, R. G. Winkler, G. Sutmann, and G. Gompper, "Semidilute polymer solutions at equilibrium and under shear flow," Macromolecules **43**, 10107–10116 (2010).
[5] J. Elgeti, U. B. Kaupp, and G. Gompper, "Hydrodynamics of sperm cells near surfaces," Biophys. J. **99**, 1018–1026 (2010).
[6] Y. Yang, V. Marceau, and G. Gompper, "Swarm behavior of self-propelled rods and swimming flagella," Phys. Rev. E **82**, 031904 (2010).
[7] A. Zöttl and H. Stark, "Hydrodynamics determines collective motion and phase behavior of active colloids in quasi-two-dimensional confinement," Phys. Rev. Lett. **112**, 118101 (2014).
[8] H. Noguchi and G. Gompper, "Dynamics of vesicle self-assembly and dissolution," J. Chem. Phys. **125**, 164908 (2006).
[9] Y. Yang, J. Elgeti, and G. Gompper, "Cooperation of sperm in two dimensions: Synchronization, attraction, and aggregation through hydrodynamic interactions," Phys. Rev. E **78**, 061903 (2008).
[10] J. Elgeti and G. Gompper, "Self-propelled rods near surfaces," Europhys. Lett. **85**, 38002 (2009).
[11] T. C. Lubensky, H. Noguchi, and G. Gompper, "Shape transitions of fluid vesicles and red blood cells in capillary flows," Proc. Natl. Acad. Sci. U. S. A. **102**, 14159–14164 (2005).
[12] T. Ihle, E. Tüzel, and D. M. Kroll, "Consistent particle-based algorithm with a non-ideal equation of state," Europhys. Lett. **73**, 664 (2006).
[13] D. H. Rothman and J. M. Keller, "Immiscible cellular-automaton fluids," J. Stat. Phys. **52**, 1119–1127 (1988).

[14]H. Noguchi and G. Gompper, "Transport coefficients of off-lattice mesoscale-hydrodynamics simulation techniques," Phys. Rev. E **78**, 016706 (2008).
[15]T. Hiller, M. Sanches de La Lama, and M. Brinkmann, "Stochastic rotation dynamics simulations of wetting multi-phase flows," J. Comput. Phys. **315**, 554–576 (2016).
[16]S. Mühlbauer, S. Strobl, and T. Pöschel, "Isotropic stochastic rotation dynamics," Phys. Rev. Fluids **2**, 124204 (2017).
[17]R. Kapral, "Multiparticle collision dynamics: Simulation of complex systems on mesoscales," Adv. Chem. Phys. **140**, 89 (2008).
[18]G. Gompper, T. Ihle, D. M. Kroll, and R. G. Winkler, "Multi-particle collision dynamics: A particle-based mesoscale simulation approach to the hydrodynamics of complex fluids," in *Advanced Computer Simulation Approaches for Soft Matter Sciences III*, edited by C. Holm and K. Kremer (Springer Berlin Heidelberg, Berlin, Heidelberg, 2009), pp. 1–87.
[19]J. T. Padding and A. A. Louis, "Hydrodynamic and Brownian fluctuations in sedimenting suspensions," Phys. Rev. Lett. **93**, 220601 (2004).
[20]I. O. Götze and G. Gompper, "Dynamic self-assembly and directed flow of rotating colloids in microchannels," Phys. Rev. E **84**, 031404 (2011).
[21]G. K. Batchelor, "Sedimentation in a dilute dispersion of spheres," J. Fluid Mech. **52**, 245–268 (1972).
[22]G. K. Batchelor, "The effect of Brownian motion on the bulk stress in a suspension of spherical particles," J. Fluid Mech. **83**, 97–117 (1977).
[23]S. H. Lee and R. Kapral, "Two-particle friction in a mesoscopic solvent," J. Chem. Phys. **122**, 214916 (2005).
[24]J. T. Padding and A. A. Louis, "Interplay between hydrodynamic and Brownian fluctuations in sedimenting colloidal suspensions," Phys. Rev. E **77**, 011402 (2008).
[25]M. Theers, E. Westphal, G. Gompper, and R. G. Winkler, "From local to hydrodynamic friction in Brownian motion: A multiparticle collision dynamics simulation study," Phys. Rev. E **93**, 032604 (2016).
[26]E. Allahyarov and G. Gompper, "Mesoscopic solvent simulations: Multiparticle-collision dynamics of three-dimensional flows," Phys. Rev. E **66**, 036702 (2002).
[27]T. Ihle and D. M. Kroll, "Stochastic rotation dynamics: A Galilean-invariant mesoscopic model for fluid flow," Phys. Rev. E **63**, 020201 (2001).
[28]E. Tüzel, M. Strauss, T. Ihle, and D. M. Kroll, "Transport coefficients for stochastic rotation dynamics in three dimensions," Phys. Rev. E **68**, 036701 (2003).
[29]J. T. Padding and A. A. Louis, "Hydrodynamic interactions and Brownian forces in colloidal suspensions: Coarse-graining over time and length scales," Phys. Rev. E **74**, 031402 (2006).
[30]J. K. G. Dhont, *An Introduction to Dynamics of Colloids* (Elsevier, 1996), Vol. 2.
[31]J. C. Crocker, "Measurement of the hydrodynamic corrections to the Brownian motion of two colloidal spheres," J. Chem. Phys. **106**, 2837–2840 (1997).
[32]J. T. Padding, A. Wysocki, H. Löwen, and A. A. Louis, "Stick boundary conditions and rotational velocity auto-correlation functions for colloidal particles in a coarse-grained representation of the solvent," J. Phys.: Condens. Matter **17**, S3393 (2005).
[33]G. G. Stokes, "On the theories of the internal friction of fluids in motion, and of the equilibrium and motion of elastic solids," Trans. Cambridge Philos. Soc. **8**, 287–319 (1845).
[34]J. M. M. Pinkerton, "A pulse method for the measurement of ultrasonic absorption in liquids: Results for water," Nature **160**, 128–129 (1947).